Closed-Form Location and Orientation Estimation in Optical Wireless Systems

Dimitrios Bozanis*, Dimitrios Tyrovolas*, Vasilis K. Papanikolaou†, Sotiris A. Tegos*,
Panagiotis D. Diamantoulakis*, Christos K. Liaskos¶, Robert Schober†, George K. Karagiannidis*
*Department of Electrical and Computer Engineering, Aristotle University of Thessaloniki, 54124 Thessaloniki, Greece
e-mail: {dimimpoz, tyrovolas, tegosoti, padiaman, geokarag}@auth.gr
†Friedrich Alexander University, 91058 Erlangen, Germany, e-mail: {vasilis.papanikolaou, robert.schober}@fau.de
¶Computer Science Engineering Department, University of Ioannina, Ioannina, Greece, e-mail: cliaskos@ics.forth.gr

***Abstract*—Accurate indoor localization is crucial for enabling 6G applications, such as smart homes, augmented reality, and advanced healthcare systems. Optical wireless systems utilizing Light-Emitting Diodes (LEDs) offer centimeter-level accuracy due to their dominant line-of-sight (LoS) characteristics. However, most existing methods assume fixed and known user orientations, limiting their practical applicability in real-world scenarios with random orientations. In this paper, we propose an LED-based visible light positioning (VLP) scheme that accurately, through closed form equations, localizes users with arbitrary orientations using optical received signal strength (RSS) measurements. The proposed method achieves high localization accuracy, without requiring hardware for orientation measurements. Finally, an analytical expression for the error is derived, while Monte Carlo simulations validate the scheme's performance, highlighting the critical role of the parameters of the system in achieving accurate localization.**

***Index Terms*—Localization, Optical Wireless Communications, Visible Light Positioning, Light-Emitting Diodes**

I. Introduction

As wireless networks evolve toward sixth-generation (6G) applications, such as immersive metaverse, smart homes, and healthcare systems, accurate indoor localization has emerged as a critical performance metric [1]. While global navigation satellite systems (GNSSs) perform poorly indoors, radio-frequency (RF) alternatives (e.g., WiFi, cellular) are heavily impacted by multipath effects. To this end, optical wireless systems using Light-Emitting Diodes (LEDs) present a compelling solution for high-precision localization, offering centimeter-level accuracy due to their dominant line-of-sight (LoS) nature, thus minimal scattering effects, and their multiple inherent degrees of freedom, such as signal intensity and angular characteristics [2]. Additionally, LED-based systems can be seamlessly integrated into existing illumination infrastructure in modern environments, enhancing energy efficiency.

Numerous visible light positioning (VLP) schemes have been proposed in the past decade. The authors of [3], introduced a trilateration technique based on optical RSS measurements, achieving a positioning accuracy of 2.4 cm at a fixed height, however, its two-dimensional positioning lacked the precision required for 6G. More recently, the authors of [4] proposed a VLP system with tilted transmitters and accounting for non-LoS components leading to centimeter-level accuracy. Similarly, the authors of [5] developed a federated learning model that uses location data to optimize network performance, demonstrating how accurate localization can support communication efficiency. However, both systems [4], [5] assume a fixed receiver orientation, which does not truly depict a practical scenario. To address this, the authors of [6] utilized accelerometer-equipped users with tilted photodetectors (PDs) to estimate the user orientation, and also proposed an error-mitigation method in the orientation measurement to further improve localization robustness. However, these approaches rely on specialized accelerometer hardware, limiting their general applicability.

Existing work has shown that optical-based positioning achieves promising localization accuracy and robustness. However, most solutions assume static and known receiver orientations, limiting their effectiveness in scenarios with varying user orientations, as often required in 6G environments. To address this, machine learning-based methods [7], [8] have introduced joint position and orientation estimation via fingerprinting. While effective, these approaches are computationally complex, operate as black-box models, and are often tailored to specific environments, reducing their generalizability.

To address these challenges, we propose an LED-based optical RSS localization scheme that accurately, through closed form equations, localizes user equipments (UEs) with arbitrary orientations. Unlike existing methods, the proposed scheme eliminates the need for specialized orientation hardware while ensuring reliable position estimation through strategic LED deployment. An expression for the error is also derived, while Monte Carlo simulations validate the effectiveness of the proposed system, offering insights into the impact of system parameters, such as PDs Field-of-View (FoV) and Lambertian emission order, on localization performance.

II. System Model

Due to their reduced susceptibility to uncontrolled scattering, optical wireless systems provide several inherent degrees of freedom that can be leveraged for localization. Among the available techniques, the RSS method is an effective solution due to its simplicity and minimal hardware requirements [9]. Specifically, RSS-based localization exploits the predictable attenuation of optical signal strength over distance, correlating these values with known spatial points to estimate the distance between an LED and the UE. Optical RSS measurements

are particularly robust in indoor environments because signal attenuation follows a reliable pattern due to the strong LoS paths. In a typical setup, the UE receives signals only from a subset of LEDs, denoted as $\mathcal{I} = \{1, \ldots, I\}$, which share a LoS link with the UE. Thus, the channel gain from the i-th LED to the UE, where $i \in \mathcal{I}$, is modeled as

$$h_i = h_{i,\mathrm{L}} + h_{i,\mathrm{N}}, \tag{1}$$

where $h_{i,\mathrm{L}}$ represents the LoS component of the channel, while $h_{i,\mathrm{N}}$ accounts for non-LoS effects due to scattering. The LoS component is expressed as [10]:

$$h_{i,\mathrm{L}} = \frac{(m_l+1)A_{\mathrm{PD}}T_f}{2\pi d_{l,i}^2}\cos^{m_l}(\psi_{d,i})g_c(\psi_{a,i})\cos(\psi_{a,i}), \tag{2}$$

where m_l is the Lambertian emission order, indicating beam directionality, and $\Psi_{1/2} = \cos^{-1}\left(e^{-\frac{m_l}{\ln(2)}}\right)$ is the half-power beamwidth of the LED. $d_{l,i}$ is the Euclidean distance between the i-th LED and the UE, while $\psi_{d,i}$ and $\psi_{a,i}$ are the departure and arrival angles, respectively. Parameters T_f, A_{PD}, and g_c represent the optical filter gain, PD area, and PD concentrator gain, respectively, with $g_c(\psi_{a,i})$ given by [10]

$$g_c(\psi_{a,i}) = \begin{cases} \frac{n_c^2}{\sin^2(\Psi_{\max})}, & 0 \le \psi_{a,i} \le \Psi_{\max} \\ 0, & \psi_{a,i} > \Psi_{\max}, \end{cases} \tag{3}$$

where n_c is the refractive index of the PD and $\Psi_{\max}$ is half the FoV of the PD. In addition to the LoS component, $h_{i,\mathrm{N}}$ is affected by reflections from objects and walls, which cannot be modeled uniformly due to their different shapes and material properties. Therefore, to accurately capture optical scattering effects, reflective surfaces are divided into smaller sections that follow the Lambertian reflectance model, which assumes that light is diffusely reflected with intensity dependent on the angle of incidence [11]. Thus, by focusing on first-order reflections, since subsequent reflections experience significant signal degradation and become negligible [11], h_i^{N} can be calculated as $h_{i,\mathrm{N}} = \sum_{j=1}^{J} h_{ij}^{\mathrm{RP}}$, where J is the number of non-LoS paths, while h_{ij}^{RP} is the j-th first-order reflection path from the i-th LED given by

$$\begin{aligned} h_{i,j}^{\mathrm{RP}} = \int_{\mathcal{S}} & \frac{\rho_r(m_l+1)A_{\mathrm{PD}}T_f}{2\pi d_{r,1}^2 d_{r,2}^2}\cos^m(\phi) \\ & \times \cos(\psi_1)\cos(\psi_2)g_c(\psi)\cos(\psi)\mathrm{d}\mathcal{S}, \end{aligned} \tag{4}$$

where $d_{r,1}$ and $d_{r,2}$ are the distances between the LED to the reflecting surface and from the reflecting surface to the UE, respectively. The reflectance of the object is denoted by ρ_r, while ψ_1 and ψ_2 are the angles of incidence and reflection, respectively. Finally, $\mathcal{S}$ is the total reflective surface to account for all the infinitesimal contributions of the first-order reflection path.

III. Optical RSS-based Localization

To determine the position $U = (x_u, y_u, z_u)$ of the UE within the room, the RSSs from multiple LEDs, which transmit in different frequencies for their signals to be distinguished in the UE, can be used because the signal strength attenuation can provide valuable information about the distance. Specifically, the power $P_{r,i}$ measured at the PD of the UE from the optical signal transmitted by the i-th LED in the optical domain is given by

$$P_{r,i} = \underbrace{h_{i,\mathrm{L}}P_{o,i}}_{P_{\mathrm{LoS},i}} + \underbrace{h_{i,\mathrm{N}}P_{o,i}}_{P_{\mathrm{NLoS},i}} + P_{n,i}, \tag{5}$$

where $P_{o,i}$ is the transmitted optical power of the i-th LED, $P_{\mathrm{LoS},i}$ and $P_{\mathrm{NLoS},i}$ are the received powers from the LoS and non-LoS components, respectively, and $P_{n,i}$ denotes the power of the noise, which arises from thermal noise, dark current, and background radiation [2].

In an ideal scenario, where the channel gain is only affected by the LoS component, based on (5) the distance between the i-th LED and the UE can be calculated using (2) and the ratio $\frac{P_{r,i}}{P_{o,i}}$. In practice, however, the received power $P_{r,i}$ is also affected by the non-LoS component and noise, which introduces errors for distance estimation. Nevertheless, in optical wireless systems, the LoS component generally dominates over the non-LoS and noise components [2], which allows us to neglect the P_{NLoS} and P_n terms in (5), thus providing a good estimate of the channel gain as

$$\hat{h}_{i,\mathrm{L}} = \frac{P_{r,i}}{P_{o,i}}. \tag{6}$$

By assuming, without loss of generality, that the transmission direction of optical signals is considered to be the positive y-axis, it means that the LEDs are placed on a plane parallel to xz, i.e., $y = y_i$. Thus, the $\psi_{d,i}$ from the i-th LED located at (x_i, y_i, z_i) to the UE can be expressed as

$$\psi_{d,i} = \cos^{-1}\left(\frac{y_u - y_i}{d_{l,i}}\right). \tag{7}$$

It should be highlighted that this formulation holds also for LEDs on other planes, with the appropriate coordinates substituted in the numerator of (7) to reflect their respective direction of transmission. Thus, by substituting (6) and (7) in (2) and after algebraic manipulations, we can express the estimated distance $\hat{d}_{l,i}$ between the i-th LED and the UE as

$$\begin{aligned} \hat{d}_{l,i} = \Bigg(& \frac{P_{o,i}}{P_{r,i}} \frac{(m_l+1)A_{\mathrm{PD}}\left(\hat{y}_u - y_i\right)^{m_l}}{2\pi} \\ & \times T_f g_c(\psi_{a,i})\cos(\psi_{a,i}) \Bigg)^{1/(m_l+2)}. \end{aligned} \tag{8}$$

It should be noted that in (8), if $P_{\mathrm{LoS,i}}$ was used in place of $P_{r,i}$, the calculated distance would represent the actual value rather than an estimate, however, it is not possible to distinguish precisely which portion of the power originates from the LoS path and which from the NLoS paths. Finally, by substituting $\hat{d}_{l,i}$ with its Cartesian coordinate form and some

algebraic manipulations, (8) can be rewritten as

$$\frac{(\hat{x}_u - x_i)^2 + (\hat{y}_u - y_i)^2 + (\hat{z}_u - z_i)^2}{(\hat{y}_u - y_i)^{\frac{2m}{m_l+2}}} = \left(\frac{P_{o,i}}{P_{r,i}} \frac{(m_l+1)A_{\mathrm{PD}}}{2\pi} T_f g_c(\psi_{a,i}) \cos(\psi_{a,i})\right)^{2/(m_l+2)}. \tag{9}$$

Examining (9), it becomes clear that a system of equations is needed to determine the position of the UE. Although three variables corresponding to the coordinates of the UE are required to define its position, three equations alone are insufficient due to the non-linear nature of the system. Therefore, it has been proven in [12] that for a fixed UE orientation, a fourth equation is required to resolve these non-linearities and ensure a unique and accurate solution to the system. These four equations can be derived from the RSS measurements of four LEDs, with each LED providing an equation corresponding to its distance from the UE, as expressed in (9). However, the random orientation of the UE introduces additional complexity regarding the unknown angles $\psi_{a,i}$ from each LED. Specifically, with I LEDs, the total number of unknowns becomes $I+3$, as each LED introduces a unique angle of incidence ψ_i in addition to the unknown UE coordinates, thereby increasing the minimum number of equations needed to ensure a unique solution. Thus, it is necessary to derive additional equations to provide more information about the system variables without increasing the number of unknowns. Furthermore, the random orientation of the UE can lead to different $\psi_{a,i}$ values, which can lead to linear dependencies between the equations and make the system unsolvable. Consequently, the LEDs must be carefully placed to ensure that the equations remain linearly independent even with random $\psi_{a,i}$ values. In this context, the following lemma establishes the constraints on the LED coordinates, which depend on the UE orientation, ensuring effective localization with the minimum possible number of LEDs.

Lemma 1: The UE position can be determined using the optical RSS-based method if it has LoS links with four LEDs placed on a plane, provided that no two LEDs are equidistant from the UE when this plane is parallel to the UE plane.

Proof: According to the optical RSS-based method, the UE position can be derived by solving a system of equations based on the RSS measurements for each LED that has a LoS link with the UE. Thus, considering 4 LEDs belonging to the set $\mathcal{I}$, and without loss of generality are placed upon $y = y_i$ plane, we obtain four equations from (9), each relating the RSS value to the UE's spatial coordinates and the corresponding angle of incidence $\psi_{a,i}$. However, since this system involves seven unknown variables, i.e., the spatial coordinates of the UE and the four incidence angles $\psi_{a,i}$, we need three additional equations to determine all these unknowns. These additional equations can be derived from geometric equations between the LED positions and the UE coordinates, involving the incidence angles $\psi_{a,i}$ and the spatial arrangement of the LEDs. However, certain constraints naturally emerge through the RSS equations, restricting the possible geometric arrangements of the LEDs. Therefore, it is essential to identify these deployment constraints to ensure the system remains solvable.

To simplify our analysis and without loss of generality, we assume $y_i = 0$, which simplifies (9) to

$$\frac{(\hat{x}_u - x_i)^2 + \hat{y}_u^2 + (\hat{z}_u - z_i)^2}{\hat{y}_u^{\frac{2m}{m_l+2}}} = \left(\frac{P_{o,i}}{P_{r,i}} \frac{(m_l+1)A_{\mathrm{PD}}}{2\pi} T_f g_c(\psi_{a,i}) \cos(\psi_{a,i})\right)^{2/(m_l+2)}. \tag{10}$$

Additionally, we assume that the PD can receive the signal from 4 LEDs and that the angle of incidence $\psi_{a,i}$ from each LED is within the maximum allowable FoV, ensuring $g_c(\psi_{a,i}) \neq 0, \forall i \in \mathcal{I}$.

To express the UE coordinates as a function of the system parameters, we start by dividing (10) for $i = 1$ and $i = 2$, yielding

$$\frac{(\hat{x}_u - x_1)^2 + \hat{y}_u^2 + (\hat{z}_u - z_1)^2}{(\hat{x}_u - x_2)^2 + \hat{y}_u^2 + (\hat{z}_u - z_2)^2} = \left(\frac{P_{r,2}\cos(\psi_{a,1})}{P_{r,1}\cos(\psi_{a,2})}\right)^{2/(m_l+2)}. \tag{11}$$

It should be noted that, to perform the division of these equations, the UE must not lie on the same plane as the LEDs, i.e., $\hat{y}_u \neq 0$, as evident from (10). Moreover, to simplify the notation, we set

$$\alpha_1 = \left(\frac{P_{r,2}\cos(\psi_{a,1})}{P_{r,1}\cos(\psi_{a,2})}\right)^{2/(m_l+2)}, \tag{12}$$

and after some algebraic manipulations, we can express $\hat{y}_u$ as (14) which is shown at the top of the page. It should be noted, that since the direction of the LED transmission coincides with the positive y-axis, $\hat{y}_u$ must be a positive value, and thus, the negative root of (11) is disregarded.

Next, to express $\hat{x}_u$ as a function of the system parameters, similarly as with $\hat{y}_u$, we can divide by (10) for $i = 1$ and $i = 3$, and by substituting (14) and setting

$$\alpha_2 = \left(\frac{P_{r,3}\cos(\psi_{a,1})}{P_{r,1}\cos(\psi_{a,3})}\right)^{2/(m_l+2)}, \tag{13}$$

we obtain (15) which is given at the top of this page. Thus, by manipulating (15), $\hat{x}_u$ can be obtained as

$$\hat{x}_u = \frac{\xi_1 \hat{z}_u + \xi_3}{\xi_2}, \tag{16}$$

where ξ_1, ξ_2, and ξ_3 are shown at the top of this page in (17), (18), and (19), respectively.

Finally, to express $\hat{z}_u$ as a function of the system parameters, we divide (10) for $i = 1$ and $i = 4$, substitute (14) and (16), and then set α_3 as

$$\alpha_3 = \left(\frac{P_{r,4}\cos(\psi_{a,1})}{P_{r,1}\cos(\psi_{a,4})}\right)^{2/(m_l+2)}, \tag{20}$$

which leads to (21) which is given at the top of the next page, and by manipulating (21), we obtain (22) given at the top of the next page.

$$\hat{y}_u = \sqrt{\frac{1}{\alpha_1 - 1}\left((\hat{x}_u - x_1)^2 + (\hat{z}_u - z_1)^2 - \alpha_1\left((\hat{x}_u - x_2)^2 + (\hat{z}_u - z_2)^2\right)\right)} \tag{14}$$

$$\begin{aligned}(\hat{x}_u - x_1)^2 + (\hat{z}_u - z_1)^2 + \frac{1}{\alpha_1 - 1}\left[(\hat{x}_u - x_1)^2 + (\hat{z}_u - z_1)^2 - \alpha_1\left((\hat{x}_u - x_2)^2 + (\hat{z}_u - z_2)^2\right)\right] \\ = \alpha_2\left[(\hat{x}_u - x_3)^2 + (\hat{z}_u - z_3)^2\right] + \frac{\alpha_2}{\alpha_1 - 1}\left[(\hat{x}_u - x_1)^2 + (\hat{z}_u - z_1)^2 - \alpha_1\left((\hat{x}_u - x_2)^2 + (\hat{z}_u - z_2)^2\right)\right]\end{aligned} \tag{15}$$

$$\xi_1 = 2\left[\alpha_1(z_1 - z_2) + \alpha_2(z_3 - z_1) + \alpha_1\alpha_2(z_2 - z_3)\right], \tag{17}$$

$$\xi_2 = 2\left[\alpha_1(x_2 - x_1) + \alpha_2(x_1 - x_3) + \alpha_1\alpha_2(x_3 - x_2)\right], \tag{18}$$

$$\xi_3 = \alpha_1\left(x_2^2 - x_1^2 + z_2^2 - z_1^2\right) + \alpha_2\left(x_1^2 - x_3^2 + z_1^2 - z_3^2\right) + \alpha_1\alpha_2\left(x_3^2 - x_2^2 + z_3^2 - z_2^2\right) \tag{19}$$

$$\begin{aligned}&\left(\frac{\xi_1\hat{z}_u + \xi_3}{\xi_2} - x_1\right)^2 + (\hat{z}_u - z_1)^2 + \frac{1}{\alpha_1 - 1}\left[\left(\frac{\xi_1\hat{z}_u + \xi_3}{\xi_2} - x_1\right)^2 + (\hat{z}_u - z_1)^2 - \alpha_1\left(\left(\frac{\xi_1\hat{z}_u + \xi_3}{\xi_2} - x_2\right)^2 + (\hat{z}_u - z_2)^2\right)\right] \\ &= \alpha_3\left[\left(\frac{\xi_1\hat{z}_u + \xi_3}{\xi_2} - x_4\right)^2 + (\hat{z}_u - z_4)^2\right] + \frac{\alpha_3}{\alpha_1 - 1}\left[\left(\frac{\xi_1\hat{z}_u + \xi_3}{\xi_2} - x_1\right)^2 + (\hat{z}_u - z_1)^2\right. \\ &\quad \left.-\alpha_1\left(\left(\frac{\xi_1\hat{z}_u + \xi_3}{\xi_2} - x_2\right)^2 + (\hat{z}_u - z_2)^2\right)\right]\end{aligned} \tag{21}$$

$$\hat{z}_u = \frac{(\alpha_1 - \alpha_3)\left[x_1\left(\xi_2 x_1 - 2\xi_3\right) + \xi_2 z_1^2\right] + \alpha_1(\alpha_3 - 1)\left[x_2\left(\xi_2 x_2 - 2\xi_3\right) + \xi_2 z_2^2\right] - \alpha_3(\alpha_1 - 1)\left[x_4\left(\xi_2 x_4 - 2\xi_3\right) + \xi_2 z_4^2\right]}{2\left[(\alpha_1 - \alpha_3)(\xi_1 x_1 + \xi_2 z_1) + \alpha_1(\alpha_3 - 1)(\xi_1 x_2 + \xi_2 z_2) - \alpha_3(\alpha_1 - 1)(\xi_1 x_4 + \xi_2 z_4)\right]} \tag{22}$$

Since we have now expressed the UE coordinates as functions of the system parameters, some constraints naturally arise regarding the LED positions. In more detail, based on (14) it, must hold that $\alpha_1 \neq 1$, which translates to

$$\frac{\cos(\psi_{a,1})}{P_{r,1}} \neq \frac{\cos(\psi_{a,2})}{P_{r,2}}. \tag{23}$$

Furthermore, from (16), we can observe that ξ_2 must not be 0, which only holds when at least 3 out of 4 LEDs do not have the same x coordinate, since $a_j > 0$, $j \in \{1, 2, 3\}$. To address these constraints regarding the identical x coordinate, (15) should be solved for $\hat{z}_u$ rather than $\hat{x}_u$, thereby shifting the constraint to the z coordinate of the LEDs instead.

Finally, to ensure that the system can be solved, the denominator of (22) can also not be equal to 0. More specifically, by taking into account that $a_1 \neq 1$, $\xi_2 \neq 0$, then to assure that the denominator in (22) is not zero, it must hold that $a_1 \neq a_3$ and $a_3 \neq 1$. Therefore, after some algebraic manipulations, the constraints mentioned above can be rewritten as

$$\frac{\cos(\psi_{a,2})}{P_{r,2}} \neq \frac{\cos(\psi_{a,4})}{P_{r,4}}, \tag{24}$$

and

$$\frac{\cos(\psi_{a,1})}{P_{r,1}} \neq \frac{\cos(\psi_{a,3})}{P_{r,3}}. \tag{25}$$

From constraints (23), (24), and (25), it can be derived that the system can be solved if and only if the distances from the LEDs, which are located on a plane parallel to the UE plane, to the UE are not equal. To prove that, these constraints must be expressed as functions of the distances between the LEDs and the UE for the case where the UE is parallel to the LEDs. Due to the planes being parallel, the angles $\psi_{d,i}$ are equal to $\psi_{a,i}$, thus, we can calculate the ratio of the received powers, appeared on (23), (24), and (25), as a function of the distances from each LED, by substituting $\psi_{a,i}$ with (7), and then by solving (8) for $P_{r,i}$. Thus, by dividing (23), (24), and (25) pairwise and performing algebraic manipulations, the constraints can be rewritten as

$$d_{l,i} \neq d_{l,j}, \forall i \neq j. \tag{26}$$

Thus, from (26) we can determine that the LEDs that are parallel to the UE must not have equal distances from the UE, which concludes the proof. ■

Remark 1: According to the proof of Lemma 1, certain LEDs may be unsuitable for UE localization at specific UE positions and orientations. To address this, it is essential to strategically place multiple LEDs in different locations, ensuring that the UE can always perform accurate localization regardless of its position or orientation.

By appropriately placing the LEDs according to Lemma 1, we can obtain geometric equations that relate the LED positions to the ratio between the cosines of the angles of incidence from each LED, and thus are able to solve the system of equations.

In this direction, a way to deploy them that satisfies these constraints is to place them all at the same height, i.e., $z = z_{\mathrm{L}}$. More specifically, this arrangement satisfies the constraint of not having LEDs with the same x coordinate, while it also gives the freedom to choose different distances between the LEDs on the x axis, making the system more tolerant of potential equalities in the distances between the LEDs and the UE. Therefore, in the following proposition, we derive the UE coordinates for the case where the LED positions coincide with the points $\mathrm{A} \equiv (x_{\mathrm{A}}, 0, z_{\mathrm{L}})$, $\mathrm{B} \equiv (x_{\mathrm{B}}, 0, z_{\mathrm{L}})$, $\mathrm{C} \equiv (x_{\mathrm{C}}, 0, z_{\mathrm{L}})$, and $\mathrm{D} \equiv (x_{\mathrm{D}}, 0, z_{\mathrm{L}})$.

Proposition 1: If the optical RSS-based method is used and the LED positions coincide with the points A, B, C, and D, the estimated UE coordinates $(\hat{x}_u, \hat{y}_u, \hat{z}_u)$ can be calculated by (16), (14), and (22), with α_1, α_2, and α_3 given by

$$\alpha_1 = \left(\frac{P_{r,2}}{P_{r,1}}\right)^{2/(m_l+1)}, \tag{27}$$

$$\alpha_2 = \left(\frac{P_{r,3}}{P_{r,1}}\right)^{2/(m_l+1)}, \tag{28}$$

$$\alpha_3 = \left(\frac{P_{r,4}}{P_{r,1}}\right)^{2/(m_l+1)}. \tag{29}$$

Proof: By expressing the incidence angles from the triangles formed between the LEDs, the UE, and the normal to the UE vector, the following expressions can be derived:

$$\hat{d}_{l,1}\cos(\psi_{a,1}) = \hat{d}_{l,2}\cos(\psi_{a,2}), \tag{30}$$

$$\hat{d}_{l,1}\cos(\psi_{a,1}) = \hat{d}_{l,3}\cos(\psi_{a,3}), \tag{31}$$

$$\hat{d}_{l,1}\cos(\psi_{a,1}) = \hat{d}_{l,4}\cos(\psi_{a,4}). \tag{32}$$

Thus, utilizing (8), (12), (13) and (20), equations (30), (31), and (32) for the 4 different distances can be rewritten as (27), (28), and (29). Thus, the UE coordinates can be obtained, which concludes the proof. ■

Remark 2: For the case where all 4 LEDs utilized for localization, are placed upon a plane that is parallel to the UE plane, i.e., the angles of incidence are equal to the angles of departure, i.e., $\psi_{d,i} = \psi_{a,i}, \forall i \in \{1, 2, 3, 4\}$, it can be proved that (12), (13), and (20) do not remain functions of these angles. Therefore, the solution of the problem can be derived directly from (22), (16), and (14) without using equations (30), (31), and (32).

Considering the existence of non-LoS components and noise, it becomes clear that the UE location cannot be acquired perfectly, because the estimated UE coordinates have been calculated based on the assumption that the optical channel is only affected by the LoS component. In this direction, in the following proposition, we provide the localization error of the optical RSS-based localization method.

Proposition 2: The localization error of the optical RSS-based method can be expressed as

$$\Delta d = d_l \left(1 - \left(\frac{1}{1 + K_{\mathrm{opt}}^{-1} + \frac{P_n}{P_{\mathrm{LoS}}}}\right)^{1/(m_l+2)}\right), \tag{33}$$

TABLE I: ROOM CHARACTERISTICS

Parameter	Value
Ceiling LED 1	$(3.5, 5, 3)$
Ceiling LED 2	$(4.5, 5, 3)$
Ceiling LED 3	$(5.5, 5, 3)$
Ceiling LED 4	$(6.5, 5, 3)$

TABLE II: SIMULATION RESULT PARAMETERS

Parameter	Value
Transmit power	$P_o = 50$ mW
Noise power	$P_n = 5 \times 10^{-14}$ A^2
Optical Filter Gain	$T_f = 1$
PD Area	$A_{\mathrm{PD}} = 1$ cm^2
PD refractive index	$n_c = 1.5$

where $K_{\mathrm{opt}} = \frac{P_{\mathrm{LoS}}}{P_{\mathrm{NLoS}}}$ is the ratio of the power of the LoS and non-LoS components of the optical channel.

Proof: The localization error between the actual and estimated distance, utilizing (8), can be expressed as

$$\begin{aligned}\Delta d =& d_l - \hat{d}_l \\ =& \left(\frac{P_o(m_l+1)A_{\mathrm{PD}}\hat{y}_u^m}{2\pi} T_f g_c(\psi_a)\cos(\psi_a)\right)^{1/(m_l+2)} \\ &\times \left(\frac{1}{P_{\mathrm{LoS}}} - \frac{1}{P_r}\right)^{1/(m_l+2)}.\end{aligned} \tag{34}$$

Finally, after some algebraic manipulations in (34), then (33) can be derived, which completes the proof. ■

IV. SIMULATION RESULTS

In this section, we evaluate the performance of the scheme through simulations in a room $10\mathrm{m} \times 10\mathrm{m} \times 3\mathrm{m}$. Specifically, the positions of the LEDs are given in Table I, while the selected values for the parameters are given in Table II. To ensure an accurate evaluation, we perform a Monte Carlo simulation with 10^6 realizations of the UE location and orientation, where in each realization the coordinates of the UE are randomly chosen within $x_u \in [0, 10\,\mathrm{m}]$, $y_u \in [0.5, 5\,\mathrm{m}]$, and $z_u \in [0.5, 2.5\,\mathrm{m}]$, while the UE's elevation and azimuth angles vary within $\theta_{\mathrm{UE}} \in \left[-\frac{\pi}{4}, \frac{\pi}{4}\right]$ and $\phi_{\mathrm{UE}} \in [0, 2\pi)$, respectively. In addition, the average value of $K_{\mathrm{opt},i}$, which captures the ratio of LoS to non-LoS components based on reflections from surrounding walls and objects, is set to the same value K_{r}.

In Fig. 1, the localization error Δd is plotted as a function of K_{r} for three Lambertian emission orders, $m_l = 1$, $m_l = 2$, and $m_l = 5$ and for $\Psi_{\max} = 75°$. As K_{r} increases, Δd decreases, highlighting the improvement in accuracy with greater LoS dominance. Furthermore, higher Lambertian orders, such as $m_l = 5$, tend to produce higher localization errors at lower K_{r} due to their narrower emission patterns, which limit coverage for certain orientations. On the contrary, $m_l = 2$ provides a balanced performance, achieving lower localization errors without the limitations of an omnidirectional pattern, i.e.,

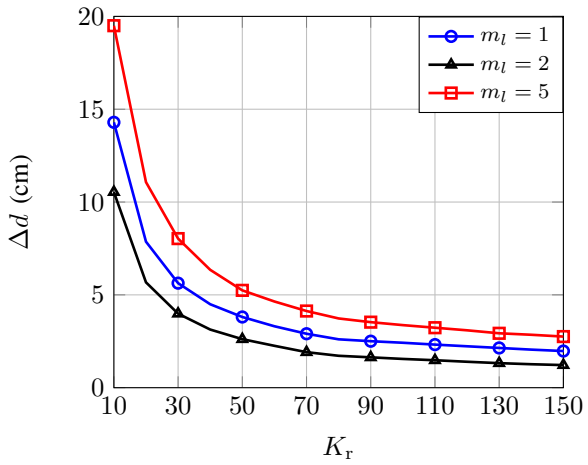


Fig. 1: Localization error Δd versus K_{r} for various m_l values.

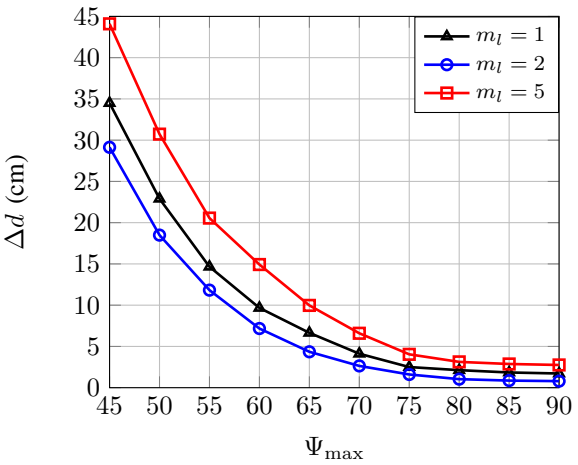


Fig. 2: Localization error Δd versus $\Psi_{\max}$ for various m_l values and for $K_{\mathrm{r}} = 100$.

$m_l = 1$, or a highly directive pattern, i.e., $m_l = 5$. However, as K_{r} continues to increase, this performance gap narrows, indicating that LoS clarity becomes the dominant factor in determining localization accuracy at high K_{r} values. To this end, Fig. 1 highlights the role of Lambertian emission order in improving localization performance.

In Fig. 2, the localization error Δd is plotted as a function of the half field-of-view (FoV) of the PD, $\Psi_{\max}$, for the same three Lambertian emission orders. As $\Psi_{\max}$ increases, Δd decreases considerably because the UE can receive signals from the LEDs over a broader angular range, leading to more accurate localization. This trend is particularly noticeable for smaller values of $\Psi_{\max}$, where the differences between the three curves are the most pronounced, highlighting the necessity for higher FoVs, especially for narrower beams. The curve corresponding to $m_l = 2$ demonstrates the best overall performance again, offering an optimal trade-off between the omnidirectional radiation pattern of $m_l = 1$ and the more directive beam of $m_l = 5$. Overall, the results emphasize the importance of carefully tuning both the PD's FoV and the Lambertian emission order to ensure accurate localization. Hence, choosing $m_l = 2$ and ensuring sufficiently wide FoV on the UE, achieves the most reliable localization.

V. Conclusion

This work proposed an LED-based optical RSS localization scheme capable of accurately localizing UEs with arbitrary orientations. By leveraging the information of LoS signal components and proposing an LED deployment to extract the position for any orientation, the proposed system provides a practical and efficient solution for indoor localization. Furthermore, a closed formula for the localization error is derived, while through Monte Carlo simulations, we demonstrated the critical role of the FoV and Lambertian emission order in achieving high localization accuracy. Finally, the results underscore the importance of strategic LED placement and system parameter tuning, offering valuable insights for the design of future 6G-compatible optical localization systems.

References

[1] A. Masaracchia, D. Van Huynh, G. C. Alexandropoulos, B. Canberk, O. A. Dobre, and T. Q. Duong, "Toward the Metaverse Realization in 6G: Orchestration of RIS-Enabled Smart Wireless Environments via Digital Twins," *IEEE Internet Things Mag.*, vol. 7, no. 2, pp. 22–28, 2024.

[2] Z. Ghassemlooy, W. Popoola, and S. Rajbhandari, *Optical Wireless Communications: System and Channel Modelling with MATLAB*, 2nd ed. CRC Press, 2019.

[3] H.-S. Kim, D.-R. Kim, S.-H. Yang, Y.-H. Son, and S.-K. Han, "An Indoor Visible Light Communication Positioning System Using a RF Carrier Allocation Technique," *J. Lightwave Technol.*, vol. 31, no. 1, pp. 134–144, Jan. 2013.

[4] N. Chaudhary, O. I. Younus, L. N. Alves, Z. Ghassemlooy, S. Zvanovec, and H. Le-Minh, "An Indoor Visible Light Positioning System Using Tilted LEDs with High Accuracy," *Sensors*, vol. 21, no. 3, p. 920, Jan. 2021.

[5] T. Wei, S. Liu, and X. Du, "Visible Light Integrated Positioning and Communication: A Multi-Task Federated Learning Framework," *IEEE Trans. Mob. Comput.*, vol. 22, no. 12, pp. 7086–7103, 2023.

[6] S. Shen, S. Li, and H. Steendam, "Hybrid position and orientation estimation for visible light systems in the presence of prior information on the orientation," *IEEE Trans. Wireless Commun.*, vol. 21, no. 8, pp. 6271–6284, 2022.

[7] M. A. Arfaoui, M. D. Soltani, I. Tavakkolnia, A. Ghrayeb, C. M. Assi, M. Safari, and H. Haas, "Invoking Deep Learning for Joint Estimation of Indoor LiFi User Position and Orientation," *IEEE J. Sel. Areas Commun.*, vol. 39, no. 9, pp. 2890–2905, 2021.

[8] Y. Huang, M. Safari, H. Haas, and I. Tavakkolnia, "Optical Wireless 3-D-Positioning and Device Orientation Estimation," *IEEE Open J. Commun. Soc.*, vol. 5, pp. 4519–4530, 2024.

[9] F. Zafari, A. Gkelias, and K. K. Leung, "A Survey of Indoor Localization Systems and Technologies," *IEEE Commun. Surv. Tutor.*, vol. 21, no. 3, pp. 2568–2599, 2019.

[10] D. Bozanis, V. K. Papanikolaou, A. A. Dowhuszko, K. G. Rallis, P. D. Diamantoulakis, J. Hämäläinen, and G. K. Karagiannidis, "Optimal Aggregation of RF and VLC Bands for Beyond 5G Mobile Services," in *Proc. 18th Int. Conf. Wireless Mobile Comput., Netw. Commun. (WiMob)*, 2022, pp. 75–80.

[11] C. Chen, D. A. Basnayaka, X. Wu, and H. Haas, "Efficient Analytical Calculation of Non-Line-of-Sight Channel Impulse Response in Visible Light Communications," *J. Light. Technol.*, vol. 36, no. 9, pp. 1666–1682, 2018.

[12] D. Bozanis, N. G. Evgenidis, V. K. Papanikolaou, P. S. Bouzinis, S. A. Tegos, A. A. Dowhuszko, P. D. Diamantoulakis, and G. K. Karagiannidis, "Indoor 3D Visible Light Positioning Analysis with Channel Estimation Errors," in *Proc. 30th Int. Conf. Systems, Signals Image Process. (IWSSIP)*, 2023, pp. 1–4.